1

Self-Standing Graphene Sheets Prepared with Chemical Vapor Deposition and Chemical Etching

Genki Odahara[1] et al. *
[1]*Department of Applied Physics, Waseda University, Tokyo, Japan*

1. Introduction

Recently, much attention has turned to the structural and electronic properties of carbon-based materials. At present, especially, graphene is the hottest topics in condensed-matter physics and materials science. This is because graphene has not only unusual properties regarding extreme mechanical strength, thermal conductivity and 2-diemensional films, but also peculiar electronic characteristics such as Dirac-particles with a linear dispersion, transport energy gap and simply absorption coefficient of lights (Geim & Novoselov, 2007; Nair et al., 2008). These unique properties mean it could have a wide array of practical uses. In addition to monolayer graphene, few-layer graphene has been extensively studied. For example, bi-layer graphene creates a band gap when an external electric field is applied (Castro et al., 2007; Zhang et al., 2009).

Graphene sheets have been produced mainly by exfoliating graphene flakes from bulk graphite and depositing them on the SiO_2/Si substrate. However, the size and crystalline quality are not easily controlled. Some groups have grown epitaxially graphene sheets on SiC(0001) (Hibino et al., 2010), however the graphene layers have been widely distributed in thickness.

For last 20 years, on the other hand, we have grown graphene (and/or h-BN), hetero-epitaxial sheets on various solid surfaces by chemical vapor deposition (CVD) or surface segregation techniques, and investigated their atomic, electronic and phonon structures (Oshima & Nagashima, 1997).

Fig. 1 shows a schematic diagram of growing processes of graphene and h-BN films by CVD or surface segregation techniques on solid surfaces reported so far. We demonstrated that the thickness of graphene, and the width of graphene nano-ribbons were controlled precisely by adjusting the annealing temperature, exposure time of deposition gases and choosing the substrate (Nagashima et al., 1994; Tanaka et al., 2002).

* Tsuyoshi Ishikawa[1], Kazuya Fukase[1], Shigeki Otani[2], Chuhei Oshima[1], Masahiko Suzuki[3], Tsuneo Yasue[3] and Takanori Koshikawa[3].
1 Department of Applied Physics, Waseda University, Tokyo, Japan,
2 National Institute for Materials Science, Tsukuba-shi, Ibaraki, Japan,
3 Fundamental Electronics Research Institute, Academic Frontier Promotion Center, Osaka Electro-Communication University, Osaka, Japan.

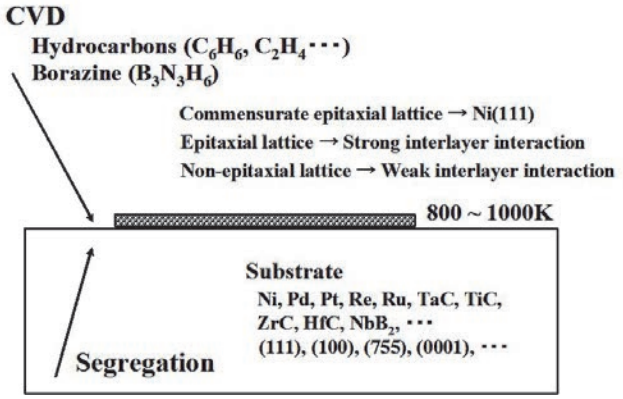

Fig. 1. A schematic diagram of growing processes of graphene and h-BN films by CVD or surface segregation techniques on solid surfaces.

Fig. 2 shows a intensity peak ratio of XPS C1s to Ta 4p as a function of hydrocarbon exposure during the graphene growth on TaC(111) (Nagashima et al., 1994). For the first monolayer formation, an exposure of a few hundred langmuir (1L = 1×10^{-6} Torr sec) was required. In comparison with the first monolayer formation, an extremely large exposure of ~8×10^5 L was necessary for the second layer growth, and the growth rate of the third layer was much slower than that of the second one. This indicates that surface reactivity for hydrocarbon dissociation is reduced at each stage of the formation of graphene overlayer.

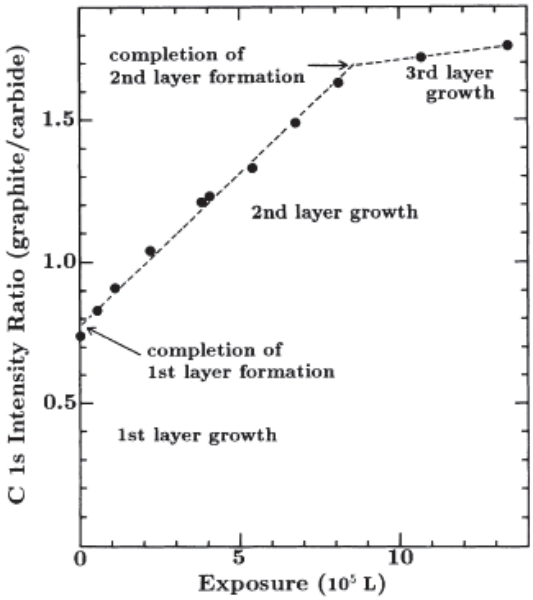

Fig. 2. An intensity peak ratio of XPS C1s to Ta 4p as a function of exposure during the graphene growth on TaC(111).

Because of the large difference in the growth rate, the thickness of the overlayer could be precisely controlled by adjusting the exposure.

Fig. 3 shows typical low energy electron diffraction (LEED) patterns of monolayer graphene and monolayer h-BN films on single-crystal surfaces. Depending on the interlayer interactions between graphene and the substrate, three different configurations were known.

1. On Pt (111), the crystallographic orientations of the growing graphene does not align with those of the substrate lattices because of the weak interlayer interaction (Fujita et al., 2005). Fig 3 (a) shows the presence of diffraction ring segments, which indicate rotational disorder of graphene domains.
2. On TaC (111), ZrC (111), Ni (100), Ni (755) and Pd (111), the incommensurate epitaxial sheets grew because of the strong interlayer interaction; there are many extra diffraction spots in the LEED patterns owing to the multiple diffraction with two different periodicity in Fig. 3 (b) and (c) (Aizawa et al., 1990; Nagashima et al., 1993a, 1993b).
3. The exception is a graphene (or h-BN)-covered Ni (111) surface; a 1 x 1 atomic structure appeared in the LEED pattern in Fig. 3 (d) and (e), because of the small lattice misfits and the strong interlayer interaction: The graphene (or h-BN) grew in a commensurate way to the substrate lattice by expanding the C-C bonds by 1.2% (by contracting the B-N bonds by 0.4%) (Gamo et al., 1997a, 1997b).

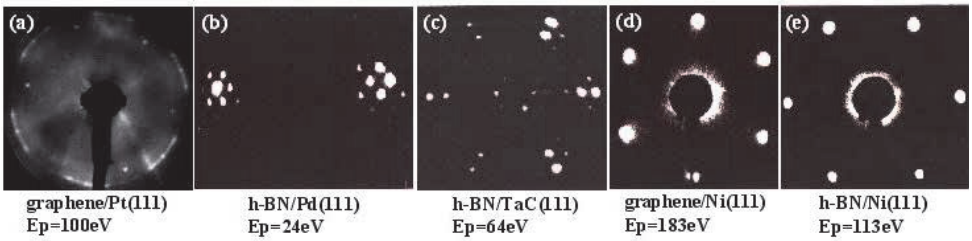

Fig. 3. Typical LEED patterns of graphene and h-BN films on single-crystal surfaces. Epitaxial films grew in a commensurate way to the Ni(111), and in incommensurate ways to the other surfaces.

Fig. 4 shows the atomic structure of the graphene-covered Ni(111) clarified with a LEED intensity analysis (Gamo et al., 1997a). The LEED intensity analysis indicated that one C atoms of graphene situate at all the on-top site of the topmost Ni atoms, and at all the three-fold FCC hollow sites. Hence, the grain boundaries of graphene islands disappeared if the surface is completely covered with either graphene or h-BN. In fact, uniform scanning tunneling microscopy (STM) images were observed on the h-BN-covered Ni(111) (Kawasaki et al., 2002).

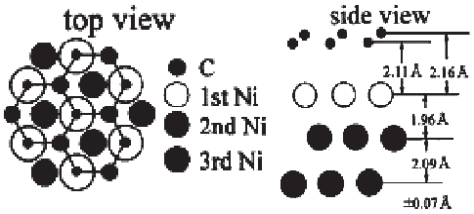

Fig. 4. The atomic structure of the graphene-covered Ni(111) clarified with a LEED intensity analysis.

Recently, we have studied the growth mechanism of graphene layers on Ni(111) surface.
In this chapter, we report the in-situ observation of the graphene growth of mono-, bi- and tri-layers using carbon segregation phenomena on Ni(111) by low energy electron microscopy (LEEM), which is a powerful technique to investigate thin films in mesoscopic scale.
We also fabricated the self-standing graphene sheets by chemically etching the substrate (Odahara et al., 2009). The chemical process to remove the Ni substrate makes it possible to prepare a self-standing graphene sheets, which are characterized by scanning electron microscopy (SEM) or transmission electron microscopy (TEM).

2. In-situ observation of graphene growth on Ni(111)

Graphene growth of mono-, bi- and tri-layers on Ni(111) through surface segregation was observed in situ by LEEM (Odahara et al., 2011). The carbon segregation was controlled by adjusting substrate temperature from 1200 K to 1050 K. After the completion of the first layer at 1125 K, the second layer grew at the interface between the first-layer and the substrate at 1050 K. The third layer also started to grow at the same temperature, 1050 K. All the layers exhibited a 1 x 1 atomic structure. The edges of the first-layer islands were straight lines, reflecting the hexagonal atomic structure. On the other hand, the shapes of the second-layer islands were dendritic. The edges of the third-layer islands were again straight lines similar to those of the first-layer islands. The phenomena presumably originate from the changes of interfacial-bond strength of the graphene to Ni substrate depending on the graphene thickness. No nucleation site of graphene layers was directly observed. All the layers expanded out of the field of view and covered the surface. The number of nucleation sites is extremely small on Ni(111) surface. This finding might open the way to grow the high quality, single-domain graphene crystals.

2.1 Macroscopic single-domain monolayer graphene sheet on Ni(111)

The carbon segregation on Ni(111) surface to grow graphene sheets has already been investigated in detail by Auger electron spectroscopy (AES) and LEED observations (Shelton et al., 1974).
Fig. 5 shows an overview of these results. The surface carbon content in a logarithmic scale is schematically shown against the temperature. Depending on the temperature, three different surfaces are observed: surfaces covered with multilayer graphene, single-layer graphene and the bare Ni substrate without graphene. Above the first critical temperature T_{c1} = 1170 K, most carbon atoms disappear at the surface, penetrating into the Ni substrate. Below $T_{c1,}$ on the other hand, the solubility of carbon in Ni is reduced and the carbon atoms segregate to the surface, forming either single- or multi-layer graphene depending on the temperatures. Below the second critical temperature T_{c2} = 1070 K, multilayer graphene is thermodynamically stable, and single-layer graphene is stable between T_{c1} and T_{c2}. The LEED patterns of the three surfaces exhibit sharp diffraction spots representing 1×1 atomic structures, indicating that the graphene layers are commensurate with Ni(111) substrate.
The high-brightness LEEM used in this work was recently developed by Koshikawa and others; a negative electrode affinity (NEA) photocathode operating in an Extreme High Vacuum (XHV, ~10^{-10} Pa) chamber achieved high brightness of 10^7A cm^{-2} sr^{-1} (Jin et al., 2008; Suzuki et al., 2010; Yamamoto et al., 2008).

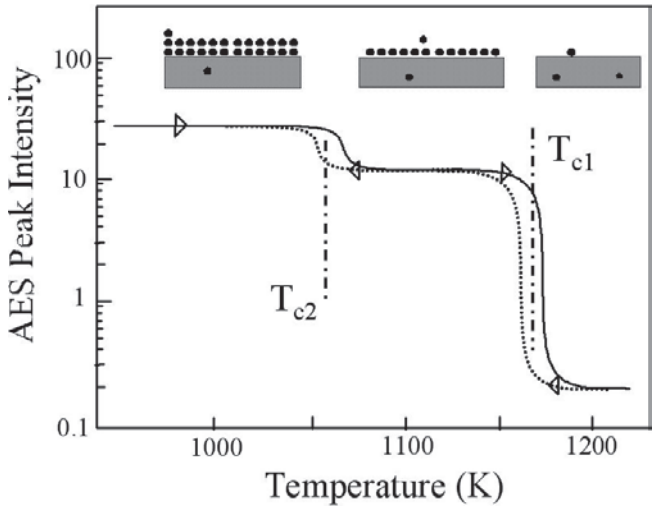

Fig. 5. Surface carbon content versus substrate temperature of a graphene-Ni(111) system (see Shelton et al., 1974). Depending on the temperature, there exist three different surfaces; multilayer coverage, monolayer coverage and bare Ni.

Fig. 6 shows snapshots from the LEEM time series after the temperature was decreased from 1200 K to 1125 K. Images (a)-(d) are 6μm field-of-view, and image (e) is 100μm field-of-view. Letters (a) to (d) in each image represents the time-lapse order during the observing period of about 3 minutes from (a) to (d). Two white domains of monolayer graphene appeared and expanded gradually as shown in images (a)-(b) and met each other in images (c)-(d). We can see clearly the straight lines at the island edges, which cross with each other by either 60° or 120° reflecting the hexagonal structure of graphene. Correctly describing, the angles are not exactly 60° and 120°, because the graphene sheets are not perfectly flat and curved along the substrate surface. Graphene sheet grew continuously across the steps in carpet-like fashion, and slightly curved at the steps.

Growing directions of graphene islands were always perpendicular to the linear edges independent of the surface structures; the Ni(111) substrate surface possesses steps with a few nm amplitudes produced by polishing as seen clearly in image (e). The graphene sheets grew continuously beyond the steps.

In images (c)-(d), they were united to form one graphene sheet without any grain boundaries. Finally, the observed area was entirely covered with monolayer graphene. We observed carefully whole the substrate surface of several centimeters in scale, but no grain boundaries were found by LEEM.

All the μLEED patterns observed in the graphene-covered surface showed a 1 x 1 structure as shown in image (f). The graphene sheets were flat and epitaxial on the terraces. The orientation was slightly altered at the steps because of the slight curving of the graphene sheet. It is strong contrast to the fact that the μLEED patterns of the bare substrate exhibited sharp diffraction spots without streaks. Namely, single-domain epitaxial sheet grew continuously across the steps. The slight streak in the μLEED pattern in image (f) reflects the curving at the steps.

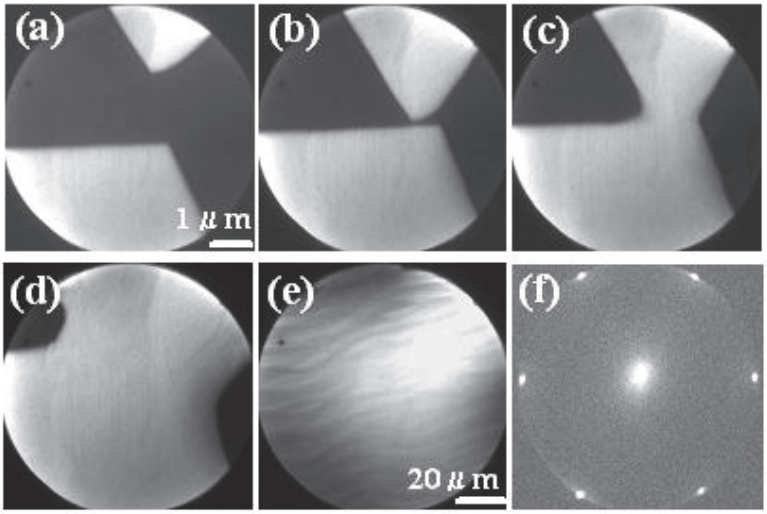

Fig. 6. Typical snapshots of LEEM images obtained as the temperature was decreased from 1200 K to 1125 K (images (a) to (d)). The observed area was 6μm field-of-view. Letter in each image indicates the time-lapse order. Two graphene domains were united to form one graphene sheet. Image (e) is a typical LEEM image of 100μm field-of-view. The surface was entirely covered with monolayer graphene. LEEM images were obtained at the primary electron energy of 3.5 eV. Image (f) is a typical μLEED pattern observed in the graphene-covered surface. The orientation of the graphene was slightly altered because the sheet is curved.

In this several tenth times observation, no nucleus generation of the islands was directly observed inside the LEEM sight at the maximum field of view, 100 μm diameter. Graphene islands always appeared out of the LEEM sight. It indicated that carbon diffusion rate was high enough to find the energetically minimum positions as compared with generation of other nucleus. That is, the number of nucleation sites is extremely small on Ni(111) surface. The small number of nucleation sites is the most important factors of growing macroscopic single-domain graphene crystals. When the graphene domains met each other, defects or corrugations arise in the graphene crystals. Compared with other metals as graphene growth substrates reported so far, Ni has the large solubility of carbon, about 0.5 at % at 1000K. Due to the large solubility of Ni, carbon atoms always segregate or penetrate into the Ni bulk at 1125K. Few graphene islands, which exceed certain critical size, could continue to grow by adopting the segregated carbon atoms. This might be the crucial reason why the single-domain large graphene sheet grow on Ni(111) surface. On Ni(111) surface, as the results, graphene sheets grew larger in carpet-like fashion independent of the morphology of substrate surface from few nucleation sites. The domains were unified without boundaries and wrinkles in the growth of the first layer on Ni(111) surface.

2.2 Bi- and tri-layer graphene growth on Ni(111)

Fig. 7 shows typical LEEM images at the different stages of the graphene growth, a typical μLEED pattern obtained from the single-layer graphene-covered surface, and the electron

reflectivity-energy curves obtained from each area: (a)-(b) the first-layer growth at 1125K, (d)-(f) the second-layer growth at 1050K and (g)-(h) the third-layer growth at 1050K. In Fig.2 (a)-(b), the growth rate of the first layer was faster than those of the second and third layers. The growth rate of the first layer was about 10μm/s.

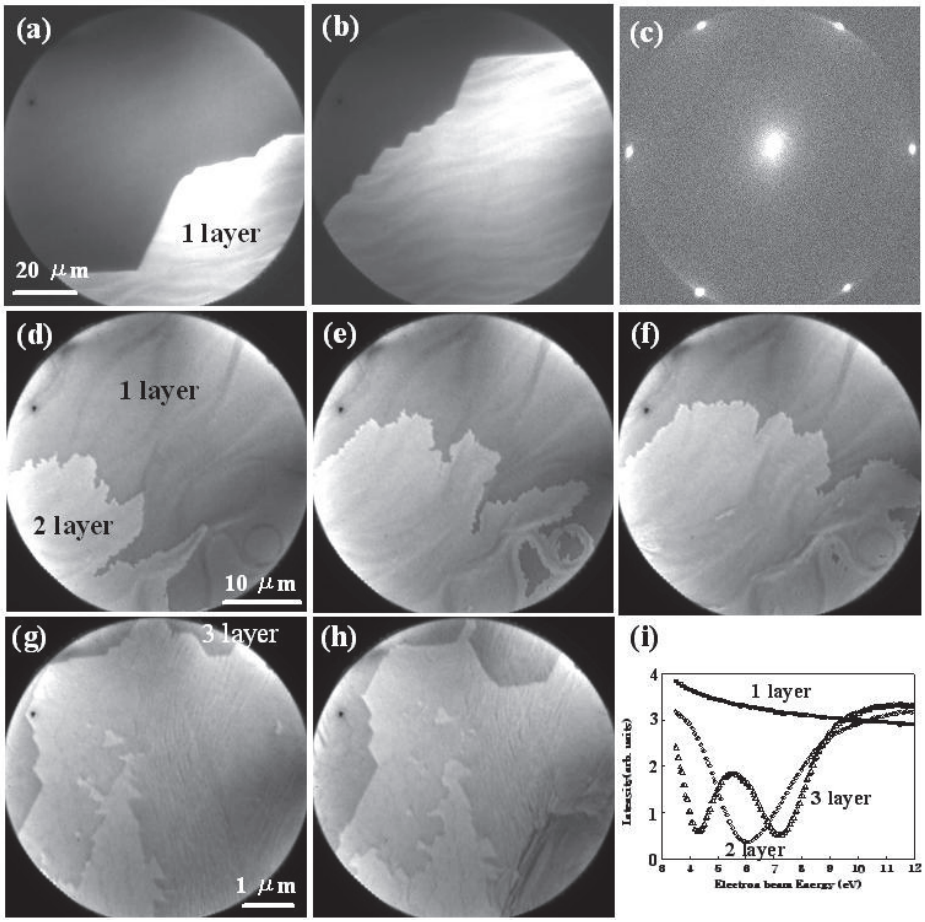

Fig. 7. Typical LEEM images of the graphene growth at different stages: (a)-(b) the first layer growth observed at 1125K, (d)-(f) the second layer at 1050K and (g)-(h) the third layer at 1050K. Image (c) is a typical μLEED pattern of a 1 x 1 atomic structure obtained from the single-layer graphene-covered surface. Image (i) is the electron reflectivity-energy curves obtained from each area.

Fig. 7 (c) is a typical μLEED pattern of a 1 x 1 atomic structure obtained from the single-layer graphene-covered surface. Similar μLEED patterns of a 1 x 1 atomic structure were obtained from the bi- and tri-layer graphene-covered surface, showing the epitaxial sheets. After the growth of the first layer was completed, we decreased the temperature from 1125 K to 1050 K to grow the second and third layers. Differing from the smooth edge of the first-

layer islands, the shape of the second-layer shown in Fig.7 (d)-(f) was dendritic; namely, the shape was determined kinetically owing to the anisotropic carbon diffusion depending on the morphology of substrate surface. The second layer grew preferentially along the morphology of the Ni substrate because of the different interfacial space owing to the first layer curving: The interfacial interaction of the first layer is stronger than the Van-der-Waals bonds in bulk graphite crystals, and the second layers have to cut into the interface between the first layer and the substrate to grow. This might be the reason of the slow-growth rate of the dendritic islands. The growth rate was about 10 times slower than that of the first layer; the growth rate of the second layer is about 1 μm/s. The second-layer grew also in carpet-like fashion independent of the morphology of substrate surface. In addition, like the first-layer growth, no nucleus generation of the second-layer islands was found even in the maximum 100 μm field-of-view. The second-layer domains always appeared out of the LEEM sight. The second-layer domains were also unified without boundaries and wrinkles. Bi-layer graphene domains grew at least 100 μm scale at 1050 K.

The interesting phenomenon was observed concerning the growth of the third layer, when we kept the temperature at 1050 K. The third layer also started to grow at a few places as shown in Fig.7 (g)-(h). The shape of the islands reflects the hexagonal atomic structure. Namely, straight lines of the island edges crossed with each other by 120°, similar to the first-layer growth. However, the growth rate is not so fast compared with that of the first-layer growth. The growth rate of the third layer is about 0.1μm/s. The carbon diffusion rate at the interface should be slower than that on the bare Ni surface, but carbon diffusion was isotropic independent of the substrate structures. Fig. 7 (i) shows the electron reflectivity-energy curves obtained from each area. The number of graphene layers can be counted directly as the number of dips in the reflectivity. The electronic energy bands of graphene sheet are quantized with sheet thickness, and possesses valleys in the energy range of 3-9 eV of the reflection curves. The valley originates from increases in the electron transmission owing to the occupied bands of graphene sheet. The valley numbers and their energy positions are changed systematically depending on the thickness such as monolayer, bi-layer, tri-layer, etc (Hibino et al., 2010).

In previous papers, we reported the weakening of the interfacial interaction with the metal substrate by the second-layer covering the first-layer through CVD technique. For example, double-layer graphene on TaC(111) and hetero-epitaxial system (monolayer graphene/monolayer h-BN) on Ni(111) (Kawasaki et al., 2002; Nagashima et al., 1994; Oshima et al., 2000).

Fig. 8 shows typical LEED patterns of two types of surfaces: (a) a monolayer h-BN on Ni(111), and (b), (c) the double atomic layers of graphene and a monolayer h-BN on Ni(111). The pattern (c) was obtained by a CCD camera with an exposure time five times longer than that used for the patterns (a) and (b). In the pattern (a), we observed sharp diffraction spots exhibiting a 1 × 1 atomic structure. Intensive LEED spots in the pattern (b) exhibiting a 1 × 1 atomic structure, together with new weak features, which are clearly seen in the pattern (c). We observed faint rings and additional spots at the positions that are rotated by 30° from those of the Ni(111) substrate. The ring radius and positions of the additional spots agreed with the reciprocal lattice of the graphene sheets, while the graphene overlayer did not have a perfect epitaxial relation to the pristine monolayer h-BN/Ni(111); namely, the graphene overlayer had domains with different azimuthal angles. Fig. 9 shows typical tunneling dI/dV spectra of (a) h-BN/Ni(111), (b) graphene/h-BN/Ni(111) and (c) highly oriented pyrolytic graphite (HOPG). The metallic characters appeared for (a) h-BN/Ni(111) in the

spectrum reflecting the strong interfacial interaction. However, the additional graphene coverage changed the spectra to the non-linear curve at zero bias, exhibiting a feature of either semiconductor or insulator.

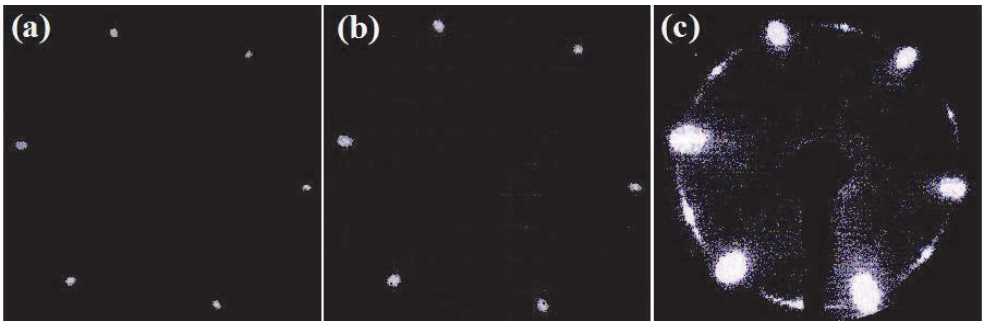

Fig. 8. Typical LEED patterns of (a) h-BN/Ni(111) and (b), (c) graphene/h-BN /Ni(111). The pattern (c) was obtained for a longer exposure, while the pattern of (B) was measured for normal exposure.

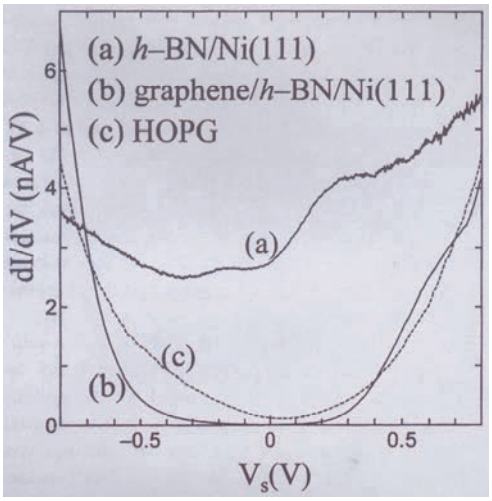

Fig. 9. Typical tunneling dI/dV spectra of (a) h-BN/Ni(111), (b) graphene/h-BN/Ni(111) and (c) HOPG. The metallic characters appeared for (a) h-BN/Ni(111).

Additional two experimental indications were observed in electronic and vibrational structures. With respect to the interfacial bonding, the first-layer graphene interacts with TaC(111) substrate, with modified π branches of electronic structure and reduced work function. Owing to the coverage of the additional second layer, the modified π branches returned to the bulk-like π branch, which indicated that interfacial interaction became weak similar to that in bulk graphite (Nagashima et al., 1994).

Another one was vibrational frequency change of phonons; the interfacial interaction reduces transverse optical (TO) frequencies of the first-layer by 20 % from the bulk ones on

Ni(111), while the additional graphene coverage returned the TO phonon frequencies to the bulk ones. All the three data described above indicated that the additional layer on the first layer weakens the interfacial interaction (Oshima et al., 2000).
The phenomenon of the third-layer growth observed by LEEM is consistent with the above data. The interfacial space of the bi- layer and substrate might not be as narrow as that of the single-layer and substrate, estimated 0.21 nm by means of LEED intensity analysis as shown in Fig. 4 (Gamo et al., 1997a). In the wide space, the segregated carbon atoms can find the energetically minimum positions similar to the case of the first-layer growth, and as a result, the equilibrium shape appeared at the third-layer growth.
We also observed interesting phenomena of moving wrinkles in the second layer growth at 1050 K, which were shown in Fig.10 . Image (a) of Fig.10 is a raw LEEM image, image (b) is the mofified image of (a) using a frame substraction method; the substraction-intensity difference between two sequent frames are protted in two dimensions in order to emphasize the moving wrinkles. We can see clearly the wave-like motions of wrinkles by eliminating the non-moving static substrate structures, which are black thick lines in image (a). Image (c) is the same image as (b) with adding the superimposed lines, which are guides for the eye indicating the moving wrinkles. The superimposed arrow indicates the direction of the second-layer growth and the smoothing direction of the wrinkles. The wrinkles moved the same direction as that of the second-layer growth. This wrinkles motions appeared just after the formation of the second layer, and the wrinkles disappeared gradually, which means that the origion of the wrinkles was stress relaese generated by the formation of the second layer, such as the mismach of lattice constant, stacking and change in the interfacial interaction between graphene and Ni(111). This phenomena are related with the motions of whole the large garphene sheet, which means that carpet-like growth occurs in the wide areas.

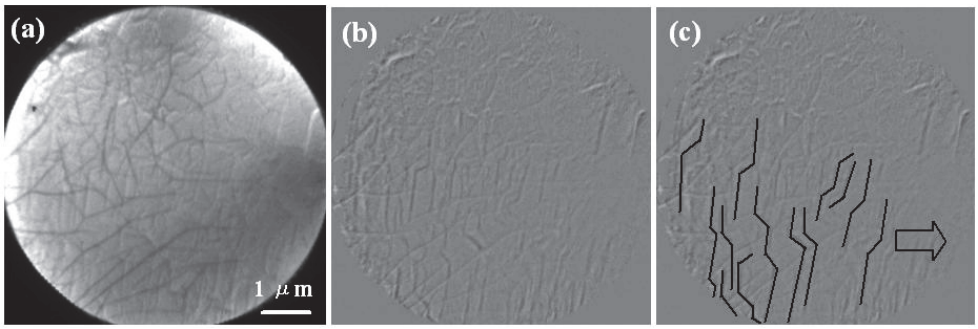

Fig. 10. A typical smoothing in the second layer growth at 1050 K. Image (a) is a raw LEEM image, (b) is the same image as (a) using frame difference method to emphasize the moving wrinkles, and remove the static substrate structures (black thick lines in image (a)). Image (c) is the same image as (b) added the superimposed lines. The superimposed arrow indicates the direction of the second-layer growth and the smoothing direction of the wrinkles.

Fig. 11 shows the mean-square amplitudes of thermal atomic vibrations of graphite(0001) surface as a function of electron energy, which were obtained from Debye-Waller factors measured on the basis of the temperature dependence of LEED intensity (Wu et al., 1985).

With decreasing the incident electron energy, the atomic vibration amplitudes became larger due to the high sensitivity of the graphite surface. This indicates that the thermal vibrational amplitudes of surface atoms are larger than that of the bulk crystal interior. However, the surface phonon dispersion curves of graphite measured with HREELS are almost the same in bulk. Hence, only the origin of the large vibrational ampulitude indicated by LEED is attributed to the phonons at long wavelength as comapred with atomic distance. These phonons cannot be detected by HREELS because their wave vectors are too small around Γ point, and their vibrational energires are too low . That is to say, whole the surface sheet moves largely, which is in good agreement with the direct observations of wrinkle motion. We concluded that the second-layer seems to grow at the interface, vibrating and stretching the wrinkles. In addition, if there are many grain boundaries in the second-layer, the wrinkle stretch easily stops at the boundaries. Since the wrinkle motion continued during the growth of the second layer, the single-domain second layer might grow in large scale.

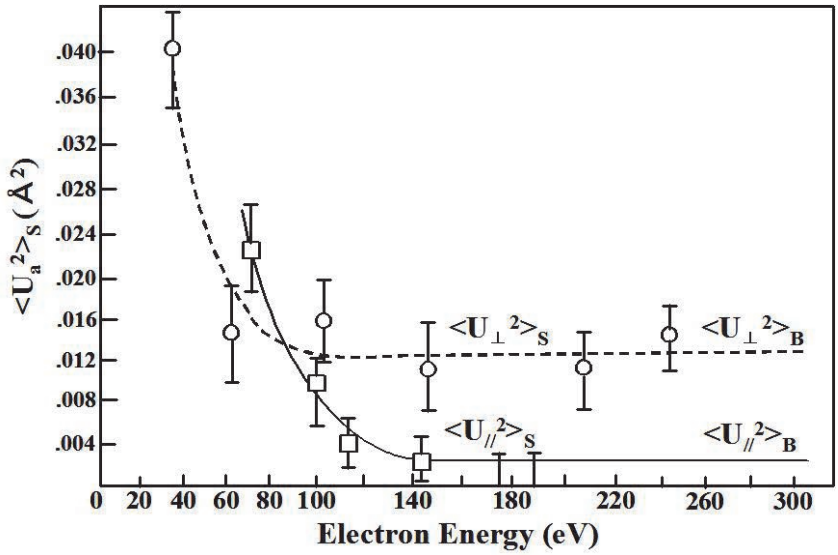

Fig. 11. The effective mean-square atomic vibration amplitudes of graphite(0001) surface as a function of electron energy (see Wu et al., 1985).

3. Self-standing graphene sheets

Additional chemically etching the Ni substrate made it possible to separate macroscopic self-standing graphene sheets with a few tenth mm in size (Odahara et al., 2009). Self-standing sheets could be the ideal sample support of organic materials for TEM observations. Low-energy electron microscope together with holder made of graphene sheets seems to be promising for observation of organic- and/or bio-materials.

Fig. 12 shows a typical TEM images (a) of the carbon aggregates at 100 kV. Because we detected only the spots of graphene sheets in diffraction patterns, we concluded that the observed materials are composed of multi-folding graphene sheets. In Fig. 12 (a), the

squares of the Au mesh are 10 μm × 10 μm in area, and the carbon aggregate in Fig. 12 (a) is a few tenth mm in scale. The magnified image of the thinnest area of the aggregate is shown in Fig. 12 (b). The uniform films covered one of the square holes of the mesh. Fig. 12 (c) is the diffraction patterns of the uniform area of Fig. 12 (b). Only sharp diffraction spots of graphene were observed, and moreover, no Ni signals were detected in X-rays analysis.

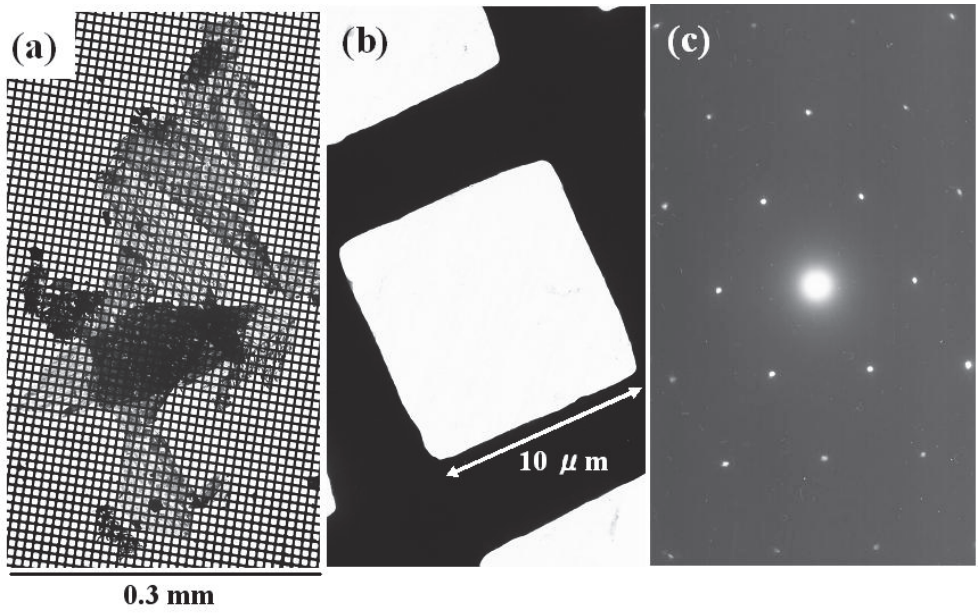

Fig. 12. (a) A TEM image of a carbon aggregate on the Au mesh with squares 10 μm × 10 μm in area, (b) A magnified TEM image of the thinnest area of the carbon aggregate, and (c) its electron diffraction pattern.

Fig. 13 shows (a) the TEM image of a slightly thicker area and (b) its diffraction pattern. All the spots are split in doublets in Fig. 13 (b). The observed area is covered with double-layer graphene sheets, of which the crystal orientations differs by 9° each others.

We saw several diffraction patterns indicating different folding structures. Hence, the double layer seems to be formed by chance during the removing the Ni substrate.

In the TEM image of the double-layer sheets, we observed CNT-like structures appeared as shown in Fig. 11 (a). The origin of the structure is not clear now.

Fig. 14 shows the 532 nm Raman spectrum of the monolayer self-standing sheets. The two intense features are the G peak at ~1580cm^{-1} and the 2D peak at ~2700 cm^{-1}. The single and sharp 2D peak in image indicates that the self-standing sheet has a thickness of only one atomic layer (Ferrari et al., 2006). In addition, small defect-origin D peak was detected at ~1350 cm^{-1}. This proves that the high-quality graphene grows on Ni(111), which could be transferred to other substrates.

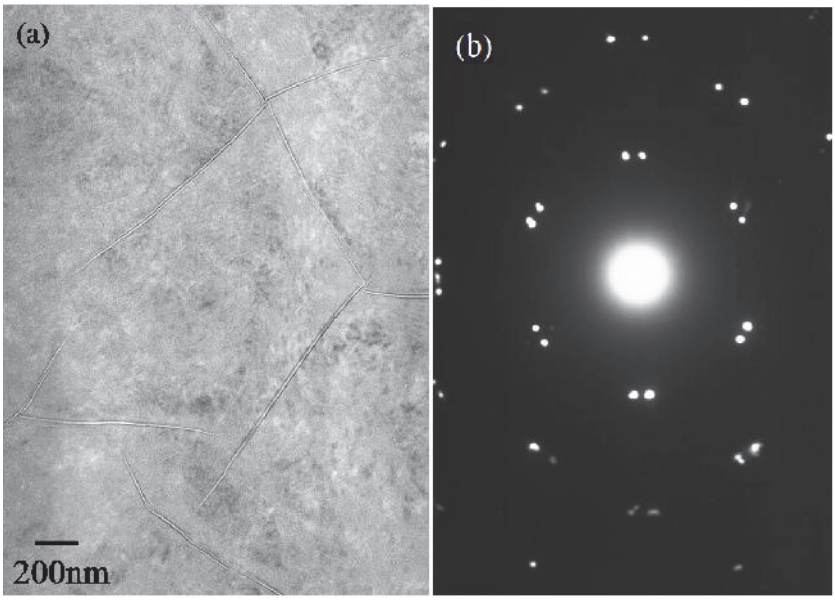

Fig. 13. A TEM image of the other area in the carbon aggregate (a) and its diffraction pattern (b). One can see clearly doublets of diffraction spots in (b), and new cabon-nano-tube like structures in (a). The hole was covered with double-layer graphene.

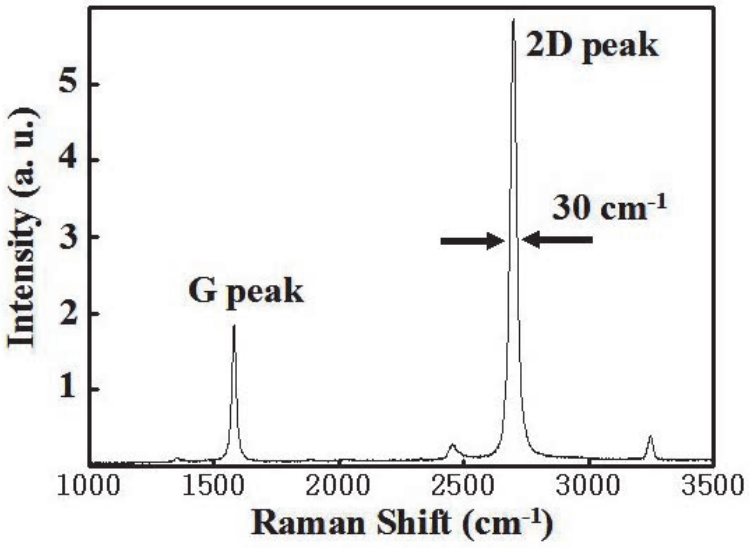

Fig. 14. Typical Raman spectrum of the monolayer self-standing graphene sheets. Small defect-origin D peak was detected at ~1350 cm^{-1}.

Lastly, we have one comment that the graphene is a promising material supporting bio-molecules for TEM observations. In Fig. 15 and Fig. 16, we showed the transmission electron diffraction patterns of a single-layer graphene measured with different electron energies of 5, 1 and 0.5 kV. With decreasing the electron energy, the ratios of diffraction spot intensity to the background intensity, and the (00) spot intensity to the (01) intensity became small, because the sensitivity of light elements change.
Fig. 15 are the SEM image of single graphene sheet at 5 kV and its Low Energy-Transmission Electron Diffraction (LETED) pattern at 5kV. Compared with TEM image, we can clearly observe the graphene surface by SEM.

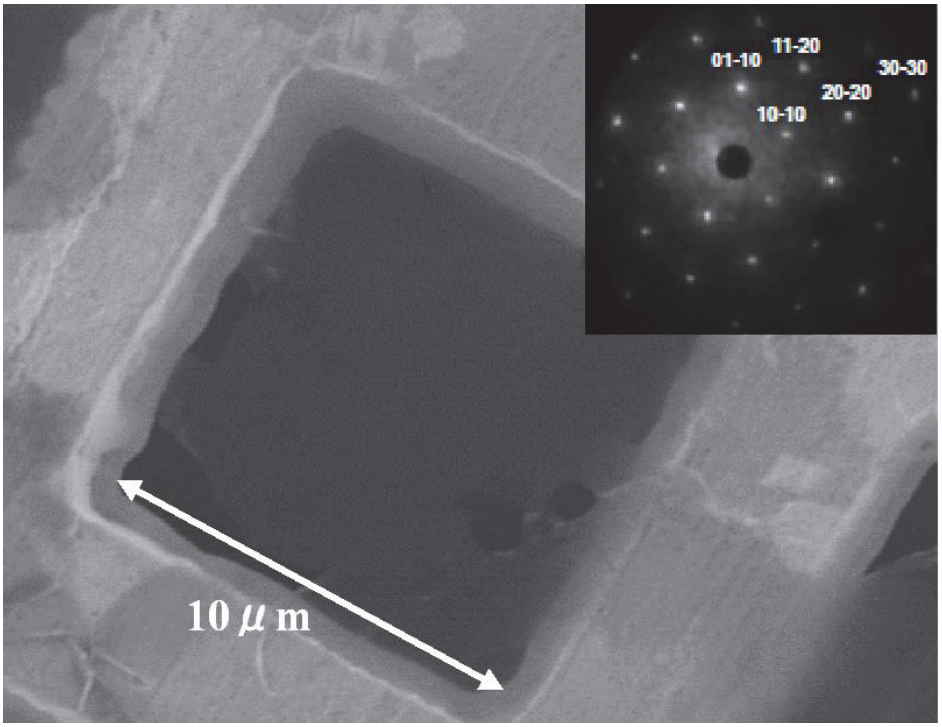

Fig. 15. The SEM image of single graphene sheet at 5 kV and its LETED pattern (upper right).

Fig. 16 shows the LETED pattern of graphene at (a) 1 kV and (b) 500 V. When we decreased the electron energy down from 1 kV to 500 V, the intensity of the (10) spot increased compared with that of the (00) spot because of large elastic scattering cross section of electrons by graphene. Adsorbed molecules on graphene sheet also increase the intensity of the diffuse scattering.
Fig. 17 is (a) the SEM image of folding double graphene sheet and its LETED pattern at (b) 4 kV and (c) 2kV. When we decreased the electron energy down from 4kV to 2kV, the additional satellite spots (white circles in image (b)) due to the double diffraction appeared in the patterns because of the large elastic scattering cross section.

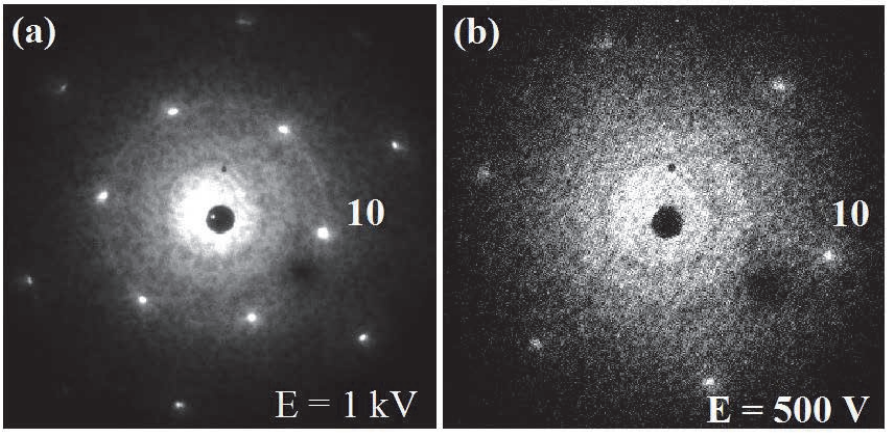

Fig. 16. The LETED pattern of single-layer graphene at (a) 1 kV and (b) 500 V.

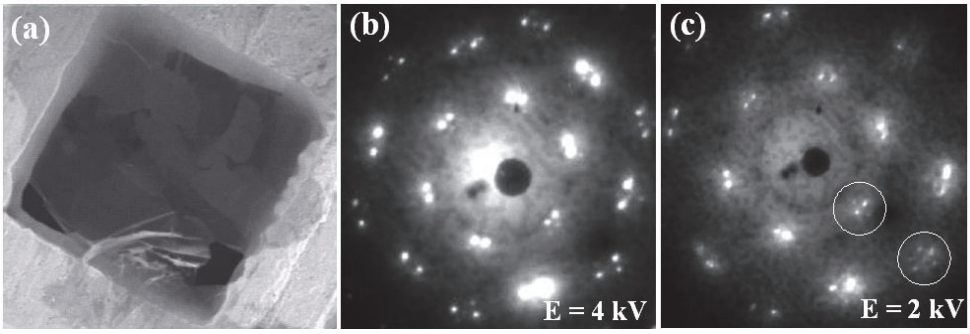

Fig. 17. The SEM image of folding double graphene sheet (a) and its LETED pattern at (b) 4 kV and (c) 2kV.

4. Conclusion

The Ni(111) surface is the excellent substrate for growth of single-layer-graphene sheet with macroscopic dimensions. Graphene sheets with a 1 x 1 atomic structure grew up epitaxially by CVD or surface segregation techniques.

We in-situ observed the graphene growth of mono-, bi- and tri-layer step by step using carbon segregation phenomena on Ni(111) by LEEM. The summaries are as follows;

1. One can grow the uniform monolayer graphene on Ni(111) by adjusting the temperature. No domain boundaries and wrinkles were detected by LEEM.
2. The second- and the third-layer graphene grew at the interface under the first and the second layers. Bi-layer graphene domains grew at least 100μm scale. The third-layer started to grow before the completion of second-layer at 1050K in this experiment. More precise control of temperature seems to be required to complete the second-layer before starting the third-layer growth.

3. Shape of the islands differed depending on the thickness; the first- and third-layer islands exhibit hexagonal edges, while the second-layer islands possess dendritic edges.
4. The different shapes of the first, second and third-layer islands presumably originate from the interfacial-bond strength depending on the graphene thickness.
5. The number of nucleation sites of graphene growth is extremely small on Ni(111) surface, which is an important factor for growth of large single-domain graphene crystals.
6. Chemical etching the Ni substrate made it possible to separate macroscopic self-standing graphene sheets.

5. Acknowledgment

M. S, T. Y and T. K are grateful for the partial support from Grants-in-Aid for Scientific Research (A) (No. 19201022).

6. References

Aizawa, T.; Souda, R.; Otani, S.; Ishizawa, Y. & Oshima, C. (1990). Anomalous bond of monolayer graphite on transition-metal carbide surfaces. *Phys. Rev. Lett.* Vol.64 pp. 768-771.

Castro, E. V.; Novoselov, K. S.; Morozov, S.V.; Peres, N. M. R.; Lopes dos Santos, J. M. B.; Nilsson, J.; Guinea, F.; Geim, A. K. & Castro Neto, A. H. (2007). Biased Bilayer Graphene: Semiconductor with a Gap Tunable by the Electric Field Effect. *Phys. Rev. Lett.* Vol.99, pp. 216802-1 - 216802-4.

Ferrari, A. C.; Meyer, J. C.; Scardaci, V.; Casiraghi, C.; Lazzeri, M.; Mauri, F.; Piscanec, S.; Jiang, D.; Novoselov, K. S.; Roth, S. & Geim, A. K. (2006). Raman Spectrum of Graphene and Graphene Layers. *Phys. Rev. Lett.* Vol.97 pp. 187401-1 - 187401-4.

Fujita, T.; Kobayashi, W. & Oshima, C. (2005). Novel structures of carbon layers on a Pt(111) surface. *Surf Interface Anal* Vol.37 pp. 120-123.

Gamo, Y.; Nagashima, A.; Wakabayashi, M.; Terai, M. & Oshima, C. (1997a). Atomic structure of monolayer graphite formed on Ni(111). *Surf. Sci.* Vol.374 pp. 61-64.

Gamo, Y.; Terai, M.; Nagashima, A. & Oshima, C. (1997b). Atomic Structural Analysis of a Monolayer Epitaxial Film of Hexagonal Boron Nitride/Ni(111) studied by LEED Intensity Analysis. *Sci. Rep. RITU* A44 pp. 211-214.

Geim, A. K. & Novoselov, K. S. (2007). The rise of graphene. *Nature Mater* Vol.6, pp. 183-191.

Hibino, H.; Kageshima, H. & Nagase, M. (2010). Epitaxial few-layer graphene: towards single crystal growth. *J. Phys. D: Appl. Phys.* Vol.43 pp. 374005 1-14.

Jin, X.; Yamamoto, N.; Nakagawa, Y.; Mano, A.; Kato, T.; Tanioku, M.; Ujihara, T.; Takeda, Y.; Okumi, S.; Yamamoto, M.; Nakanishi, T.; Saka, T.; Horinaka, H.; Kato, T.; Yasue, T. & Koshikawa, T. (2008). Super-High Brightness and High-Spin-Polarization Photocathode. *Appl. Phys. Express* Vol.1 pp. 045002-1-045002-3.

Kawasaki, T.; Ichimura, T.; Kishimoto, H.; Akber, A. A.; Ogawa, T. & Oshima, C. (2002). Double atomic layers of graphene/monolayer h-BN on Ni(111) studied by scanning

tunneling microscopy and scanning tunneling spectroscopy. *Surf. Rev. Lett.* Vol.9 pp. 1459-1464.

Nagashima, A.; Itoh, H.; Ichinokawa, T. & Oshima, C. (1994). Change in the electronic states of graphite overlayers depending on thickness. *Phys. Rev. B*, Vol.50 pp. 4756-4763.

Nagashima, A.; Nuka, K.; Itoh, H.; Ichinokawa, T. & Oshima, C. (1993). Electronic states of monolayer graphite formed on TiC(111) surface. *Surf. Sci.* Vol.291 pp. 93-98.

Nagashima, A.; Nuka, K.; Satoh, K.; Itoh, H.; Ichinokawa, T. & Oshima, C. (1993). Electronic structure of monolayer graphite on some transition metal carbide surfaces. *Surf. Sci.* Vol.287/288 pp. 609-613.

Nair, R. R.; Blake, P.; Grigorenko, A. N.; Novoselov, K. S.; Booth, T. J.; Stauber, T.; Peres, N. M. R. & Geim, A. K. (2008). Fine Structure Constant Defines Visual Transparency of Graphene. *Science* Vol.320, pp. 1308.

Odahara, G.; Ishikawa, T.; Otani, S. & Oshima, C. (2009). Self-Standing Graphene Sheets Prepared with Chemical Vapor Deposition and Chemical Etching. *e-J. Surf. Sci. Nanotech.* Vol.7 pp. 837-840.

Odahara, G.; Otani, S.; Oshima, C.; Suzuki, M.; Yasue, T. & Koshikawa, T. (2011). In-situ Observation of Graphene Growth on Ni(111). *Surf. Sci.* Vol. 605 pp. 1095-1098.

Oshima, C. & Nagashima, A. (1997). Ultra-thin epitaxial films of graphite and hexagonal boron nitride on solid surfaces. *J. Phys.: Condens. Matter* Vol.9 pp. 1-20.

Oshima, C.; Itoh, A.; Rokuta, E.; Tanaka, T.; Yamashita, K. & Sakurai, T. (2000). A hetero-epitaxial-double-atomic-layer system of monolayer graphene/monolayer *h*-BN on Ni(111). *Solid State Commun.* Viol.116 pp. 37-40.

Shelton, J. C.; Patil, H. R. & Blakely, J. M. (1974). Equilibrium segregation of carbon to a nickel (111) surface: A surface phase transition. *Surf. Sci.* Vol.43 pp. 493-520.

Suzuki, M.; Hashimoto, M.; Yasue, T.; Koshikawa, T.; Nakagawa, Y.; Konomi, T.; Mano, A.; Yamamoto, N.; Kuwahara, M.; Yamamoto, M.; Okumi, S.; Nakanishi, T.; Jin, X.; Ujihara, T.; Takeda, Y.; Kohashi, T.; Ohshima, T.; Saka, T.; Kato, T. & Horinaka, H. (2010). Real Time Magnetic Imaging by Spin-Polarized Low Energy Electron Microscopy with Highly Spin-Polarized and High Brightness Electron Gun. *Appl. Phys. Express* Vol.3 pp. 026601-1-026601-3.

Tanaka, T.; Tajima, A.; Moriizumi, R.; Hosoda, M.; Ohno, R.; Rokuta, E.; Oshima, C. & Otani, S. (2005). Carbon nano-ribbons and their edge phonons. *Solid State Commun.* Vol.123 pp. 33-36.

Wu, N. J.; Kumykov, V. & Ignatiev, A. (1985). Vibrational properties of the graphite (0001) surface. *Surf. Sci.* Vol.163 pp. 51-58.

Yamamoto, N.; Nakanishi, T.; Mano, A.; Nakagawa, Y.; Okumi, S.; Yamamoto, M.; Konomi, T.; Jin, X.; Ujihara, T.; Takeda, Y.; Ohshima, T.; Saka, T.; Kato, T.; Horinaka, H.; Yasue, T.; Koshikawa, T. & Kuwahara, M. (2008). High brightness and high polarization electron source using transmission photocathode with GaAs-GaAsP superlattice layers. *J. Appl. Phys*, Vol.103 pp. 064905-1 - 064905-7.

Zhang, Y.; Tang, T-T.; Girit, C.; Hao, Z.; Martin, M. C.; Zettl, A.; Crommie, M. F.; Ron Shen, Y. & Wang, F. (2009). Direct observation of a widely tunable bandgap in bilayer graphene. *Nature* Vol.459 pp. 820-823.